# Impact of Sodium Pyruvate on the Electrochemical Reduction of $NAD^+$ Biomimetics

Chase Bruggeman, Karissa Gregurash and David P. Hickey*

Department of Chemical Engineering and Materials Science, Michigan State University, East Lansing, MI 48824-1226

E-mail: hickeyd6@msu.edu

## ABSTRACT

Biomimetics of nicotinamide adenine dinucleotide (mNADH) are promising cost-effective alternatives to their natural counterpart for biosynthetic applications; however, attempts to recycle mNADH often rely on coenzymes or precious metal catalysts. Direct electrolysis is an attractive approach for recycling mNADH, but electrochemical reduction of the oxidized mimetic ($mNAD^+$) primarily results in the formation of an enzymatically inactive dimer. Herein, we find that aqueous electrochemical reduction of an $NAD^+$ mimetic, 1-*n*-butyl-3-carbamoylpyridinium bromide (**1**$^+$), to its enzymatically active form, 1,4-dihydro-1-*n*-butyl nicotinamide (**1H**), is favored in the presence of sodium pyruvate as a supporting electrolyte. Maximum formation of **1H** is achieved in the presence of a large excess of pyruvate in combination with a large excess of a co-supporting electrolyte. Formation of **1H** is found to be favored at pH 7, with an optimized product ratio of ~50/50 dimer/**1H** observed by cyclic voltammetry. Furthermore, sodium pyruvate is shown to promote electroreductive generation of the 1,4-dihydro form of several additional mNADH as well as NADH itself. This method provides a general strategy for regenerating 1,4-dihydro-nicotinamide mimetics of NADH from their oxidized forms.

Keywords: oxidoreductase, electrocatalysis, bioelectrocatalysis, redox mediator, supporting electrolyte, boron doped diamond, cyclic voltammetry

## INTRODUCTION

Recently there has been a significant expansion in the use of bioelectrocatalysis for environmentally friendly organic synthesis.[1] In bioelectrocatalysis, redox enzymes drive highly selective redox reactions under mild aqueous conditions, and the corresponding enzyme cofactor is regenerated with an electrode as the terminal oxidant/reductant. One cofactor, nicotinamide adenine dinucleotide (phosphate) ($NAD(P)^+$/NAD(P)H), holds special appeal for

bioelectrocatalysis, because it is used by half of documented oxidoreductases[2]; however, its commercial utilization is limited by its high cost. A promising step towards low-cost redox cofactors was demonstrated with simple NADH mimetics (mNADH), such as 1-*n*-butyl-1,4-dihydronicotinamide (**1H**), that were shown to exhibit activity with enoate reductase, hydroxybiphenyl monooxygenase, and BM3 cytochrome p450.[3–7] Both the natural cofactor, NADH, and its mimetics commonly function as hydride donors, undergoing a concerted two-electron/one-proton transfer to yield the oxidized form, $NAD^+$; however, direct electrochemical reduction of $NAD^+$ and its mimetics proceeds via sequential single electron/proton transfers. These reductions can be intercepted after the first electron transfer, with rapid formation of enzymatically inactive dimers (rate constant for dimerization exceeds $10^7$ $M^{-1}s^{-1}$).[8] The first one-electron reduction of $NAD^+$ occurs between -0.9 V and -1.2 V, and the resulting neutral pyridine radical can be further reduced near -1.6 V to form the enzymatically active 1,4-dihydropyridine (all potentials reported vs SCE).[8,9]

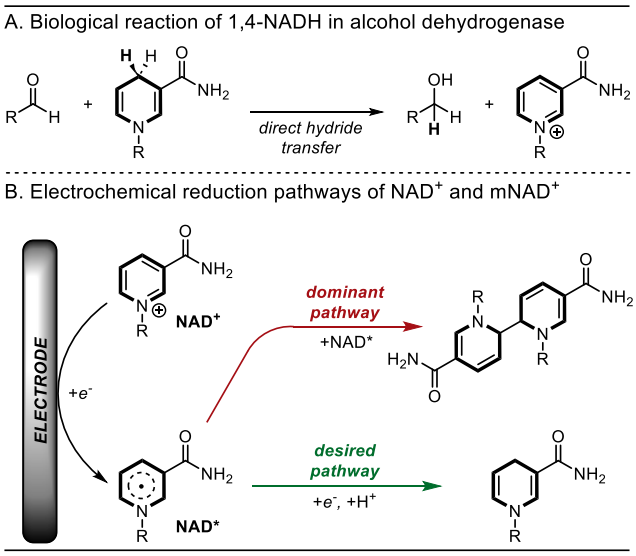


**Scheme 1.** (A) Example biological reaction involving NADH, where alcohol dehydrogenase catalyzes the reduction of an aldehyde to an alcohol. The reaction proceeds via hydride transfer. (B) Mechanism for direct electrochemical reduction of $NAD^+$. The reaction proceeds via sequential electron-proton transfer and is intercepted after the first electron to form dimer rather than the desired biologically active NADH.

In practice, however, the electrochemical yields of enzymatically-active NADH from constant potential electrolysis are near 65-76%, and no NADH is observed at moderate reduction potentials (*ca.* -1.2 V).[10] While methods do exist to optimize the yield of electrochemically

generated NADH above even 90%, for example Rh hydride-transfer catalysts[6,11] and Pt-patterned glassy carbon electrodes[12], these methods are limited by slow turnover rates and a sensitivity to the precise voltage/metal surface coverage. While the operational simplicity of direct electrochemistry and its high theoretical (m)NADH regeneration rate (limited only by mass transport) hold promise for bioelectrocatalysis, its use is still limited by the undesired dimerization reaction.

While it is known that the supporting electrolyte can play a critical role in governing the product distribution of electrochemically-coupled chemical reactions,[13–18] little attention has been given to the role of supporting electrolyte in the electrochemical reduction of $NAD^+$ or its mimetics.[19] In light of this, we considered the possibility that dimerization could be minimized in electrochemical (m)$NAD^+$ reduction through judicious choice of supporting electrolyte. We chose **1H** as a model cofactor, hypothesizing that supporting electrolyte could lower the relative rate of dimerization and increase the relative rate of **1H** formation during electrochemical reduction of the mimetic's oxidized form, 1-*n*-butyl nicotinamide bromide ($\mathbf{1^+}$). To test this hypothesis, we screened the electrochemistry of the bromide salt of $\mathbf{1^+}$ in 28 different supporting electrolytes at a boron-doped-diamond electrode, and we compared this against the electrochemistry of **1H** formed by dithionite reduction. We used cyclic voltammetry for its operational simplicity, and for the ease with which information about concentration profiles and product distributions could be extracted.

## RESULTS AND DISCUSSION

The cyclic voltammogram (CV) for 2 mM $\mathbf{1^+}$ in aqueous 200 mM sodium bicarbonate reveals an irreversible reduction peak at -1.3 V and an irreversible oxidation peak at -0.05 V (*ox1*) (all potentials reported vs SCE). The potential of *ox1* is consistent with that of a dimer formed by electrochemically generated neutral radical species of $\mathbf{1^+}$ (i.e., $\mathbf{1^*}$).[20] By contrast, CVs of the chemically prepared, pure form of **1H** result in no peak at 0 V during the initial scan, but instead a large irreversible oxidation peak is observed near 0.44 V (*ox2*) followed by a reduction peak at -1.3 V matching that of $\mathbf{1^+}$. After the first cycle, an oxidation peak consistent with *ox1* becomes visible (Figure 1). A summary of this general reaction mechanism is given by:

(1) $\mathbf{1^+} \xrightarrow{e^-} \mathbf{1^*}$

(2) $\mathbf{1^*} + \mathbf{1^*} \longrightarrow \mathbf{1_{dim}}$

(3) $\mathbf{1}^{*} \xrightarrow{H^{+}/e^{-}} \mathbf{1H}$

(4) $\mathbf{1}_{\mathbf{dim}} \xrightarrow{-e^{-}} \mathbf{1}^{*} + \mathbf{1}^{+}$ (*ox1*)

(5) $\mathbf{1H} \xrightarrow{-e^{-}} \mathbf{1}^{*} + H^{+}$ (*ox2*)

where $\mathbf{1}_{\mathbf{dim}}$ is the electrochemically dimerized mimetic. The presence of two distinct peaks corresponding to electrochemical oxidation of the dimer (*ox1*) and oxidation of the 1,4-dihydropyridine **1H** (*ox2*) provides a convenient means to measure the relative amounts of dimer and **1H** generated upon electrochemical reduction under variable conditions.

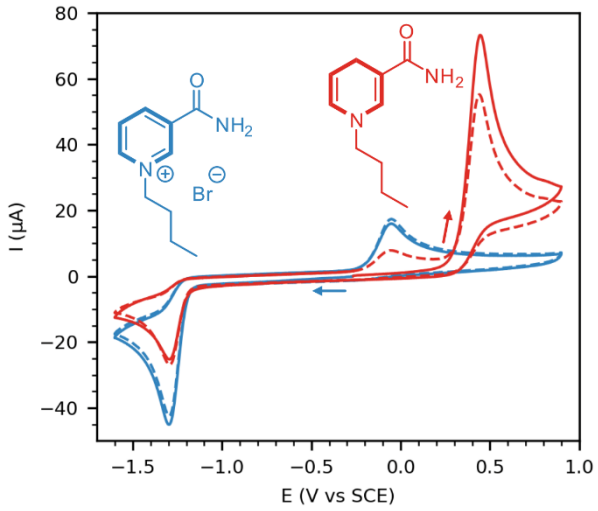


**Figure 1.** Representative cyclic voltammograms of 2 mM 1-*n*-butyl nicotinamide bromide, $\mathbf{1}^{+}$, (—) and 2 mM 1,4-dihydro-1-*n*-butyl nicotinamide, **1H**, (—). Solid curves represent the first CV scans, while dashed lines represent the second CV scans. Experiments were performed using a 2 mm boron doped diamond working electrode, saturated calomel reference electrode, and platinum wire counter electrode, with 200 mM aqueous $NaHCO_3$ purged with $N_2$ and at 25 °C and 800 mV $s^{-1}$.

To determine the impact of supporting electrolyte on the distribution of peaks corresponding to dimer and dihydro species (*ox1* and *ox2*, respectively), CVs of 2 mM $\mathbf{1}^{+}$ were performed in 28 different supporting electrolytes, including $Na^{+}$, $K^{+}$, $Li^{+}$, $Ca^{2+}$, $Mg^{2+}$, $NH_4^{+}$, or organic ammonium cations with halide, sulfate, phosphate, nitrate, carbonate, azide, or borate anions. Additionally, sodium and potassium salts of several organic anions were tested, including

acetate, citrate, oxalate, gluconate, propionate, and pyruvate. The resulting voltammograms are summarized in Table 1. For most of the electrolytes studied, $\mathbf{1}_{\mathbf{dim}}$ was the only observable reduction product. The CVs were qualitatively nearly identical with only small variations in the reduction event ($E_{pc}$ = -1.3 V, $i_{pc}$ = 35–45 μA) and moderate variations in *ox1* ($E_{pa1}$ = -0.07–0 V, $i_{pa1}$ = 11–19 μA). A small additional oxidation event ($E_{pa2}$ = 0.35 V, $i_{pa2}$ < 0.1 μA) was observed in the most acidic solutions ($NaH_2PO_4$ and $NH_4H_2PO_4$, where pH < 5), indicating a general pH dependence for the product distribution of electrochemically reduced $\mathbf{1}^+$.

| | peak current / μA | | | peak potential / V vs SCE[a] | | | |
|---|---|---|---|---|---|---|---|
| Electrolyte | $\mathbf{1}^+$ reduction | dimer oxidation (*ox1*) | **1H** oxidation (*ox2*) | $\mathbf{1}^+$ reduction | dimer oxidation (*ox1*) | **1H** oxidation (*ox2*) | pH |
| $Na_2CO_3$ | 42.5 ± 0.2 | 17.4 ± 0.1 | - | -1.295 ± 0.001 | -0.049 | - | 11.2 |
| $NaN_3$ | 43.76 ± 0.07 | 18.22 ± 0.01 | - | -1.296 | -0.056 | - | 10.1 |
| $Na_2B_4O_7$[b] | 41.35 ± 0.03 | 15.62 ± 0.06 | - | -1.307 | -0.049 | - | 9.6 |
| $K_2HPO_4$ | 41.45 ± 0.01 | 16.7 ± 0.1 | - | -1.299 | -0.036 ± 0.001 | - | 9.2 |
| $Na_2HPO_4$ | 39.7 ± 0.1 | 14.81 ± 0.05 | - | -1.305 ± 0.001 | -0.001 ± 0.001 | - | 9.1 |
| $NaHCO_3$ | 42.56 ± 0.09 | 17.41 ± 0.05 | - | -1.295 ± 0.001 | -0.052 ± 0.002 | - | 8.9 |
| $CaCl_2$ | 35.7 ± 0.2 | 13.35 ± 0.08 | - | -1.31 | 0.017 ± 0.002 | - | 8.8 |
| $(NH_4)_2HPO_4$ | 40.46 ± 0.04 | 15.14 ± 0.02 | - | -1.302 | -0.019 | - | 8.3 |
| $Na_2SO_4$ | 41.2 ± 0.1 | 16.89 ± 0.09 | - | -1.304 ± 0.001 | -0.012 ± 0.003 | - | 7.7 |
| $KNO_3$ | 43.6 ± 0.2 | 17.2 ± 0.04 | - | -1.301 ± 0.001 | -0.029 | - | 7.3 |
| LiBr | 43.2 ± 0.1 | 16.73 ± 0.09 | - | -1.296 | -0.051 ± 0.001 | - | 7.3 |
| KCl | 44.3 ± 0.2 | 16.95 ± 0.07 | - | -1.303 | -0.02 ± 0.002 | - | 7.2 |
| $MgSO_4$ | 41.1 ± 0.1 | 16.4 ± 0.02 | - | -1.299 | -0.041 | - | 7.2 |
| KBr | 43.3 ± 0.1 | 16.59 ± 0.01 | - | -1.302 ± 0.001 | -0.032 ± 0.001 | - | 7.1 |
| NaCl | 42.9 ± 0.1 | 18.06 ± 0.09 | - | -1.293 ± 0.001 | -0.056 ± 0.001 | - | 6.9 |
| NaBr | 43.78 ± 0.05 | 17.78 ± 0.01 | - | -1.301 ± 0.001 | -0.039 ± 0.002 | - | 6.6 |
| $NaNO_3$ | 42.1 ± 0.2 | 17.0 ± 0.2 | - | -1.3 ± 0.001 | -0.038 | - | 6.5 |
| $NH_4Cl$ | 44.57 ± 0.02 | 16.31 ± 0.02 | - | -1.307 ± 0.001 | 0.000 ± 0.001 | - | 6.2 |
| $NH_4H_2PO_4$ | 40.9 ± 0.1 | 11.92 ± 0.02 | 0.04 | -1.312 | 0.012 ± 0.003 | 0.35 ± 0.002 | 4.7 |
| $NaH_2PO_4$ | 38.3 ± 0.2 | 10.88 ± 0.03 | 0.07 | -1.303 | -0.025 ± 0.001 | 0.35 ± 0.001 | 4.6 |
| NaCitrate | 42 ± 0.2 | 16.4 ± 0.2 | - | -1.304 ± 0.001 | -0.036 ± 0.001 | - | 8.9 |
| $K_2C_2O_4$ | 44.49 ± 0.03 | 18.1 ± 0.1 | - | -1.301 | -0.033 ± 0.001 | - | 7.8 |
| $Bu_4NBr$ | 38.1 ± 0.2 | 14.42 ± 0.04 | - | -1.283 | -0.001 ± 0.001 | - | 7.2 |
| $Pr_4NBr$ | 39.3 ± 0.2 | 15.21 ± 0.03 | - | -1.289 | -0.025 ± 0.001 | - | 7.2 |
| NaPyruvate | 44.29 ± 0.07 | 12.66 ± 0.01 | 4.4 ± 0.1 | -1.314 | -0.008 ± 0.001 | 0.489 ± 0.002 | 7.0 |
| NaAcetate | 41.2 ± 0.1 | 15.39 ± 0.09 | - | -1.309 ± 0.001 | -0.039 | - | 6.9 |
| NaPropionate | 38.88 ± 0.05 | 14.85 ± 0.02 | - | -1.309 | -0.025 ± 0.002 | - | 6.7 |
| K-(D)-Gluconate | 40.7 ± 0.2 | 15.38 ± 0.05 | - | -1.303 | -0.037 ± 0.003 | - | 6.7 |

**Table 1.** CV output data from inorganic (top) and organic (bottom) electrolytes tested with $\mathbf{1}^+$, including the peak currents and peak potentials for $\mathbf{1}^+$ reduction, $\mathbf{1}_{\mathbf{dim}}$ oxidation (*ox1*), and **1H** oxidation (*ox2*). Values are reported as the average and one standard deviation with $n$ = 3. Experiments were performed using 2 mM 1+ with 200 mM supporting electrolyte purged with $N_2$ and at 25 °C and 800 mV $s^{-1}$. [a] Unless otherwise noted, the standard deviation for a given peak potential was less than 1 mV. [b] 100 mM Sodium tetraborate decahydrate was used.

Among the electrolytes tested, sodium pyruvate stood out for its ability to promote **1H** formation, even at neutral pH ($E_{pa2}$ = 0.49 V, $i_{pa2}$ = 4 μA at pH 7.0). To better understand the unique effect of sodium pyruvate on the electrochemistry of $\mathbf{1}^+$, we used convolution voltammetry to compare the product distributions in the presence and absence of pyruvate (see Supporting Information for a brief description of convolution voltammetry).[21,2223] Convolution voltammetry shows the effective concentration change of a redox-active substrate at the electrode surface, assuming that the substrate participates only in diffusion and electron transfer. The height of the convolution integral is proportional to the number of electrons transferred per molecule. Figure 2 shows CVs (top, solid curves) and convolution integrals (bottom, dashed curves) of $\mathbf{1}^+$ at pH 7, in 100 mM sodium phosphate (blue) and in 100 mM sodium phosphate plus 100 mM sodium pyruvate (red). Both graphs show the appearance of *ox2* when sodium pyruvate is added. The convolution integral, when normalized for a one-electron reduction (Figure 2B), shows that the concentration of $\mathbf{1}^+$ drops by 2 mM (i.e., the bulk concentration) when reduced without sodium pyruvate, and that it returns to the bulk concentration after *ox1*. By contrast, the effective concentration change with sodium pyruvate is over 4 mM after the reduction event. Part of this change is attributable to the change in mechanism, from a one-electron reduction ($\mathbf{1}^+$ to $\mathbf{1}_{\mathbf{dim}}$) to a two-electron reduction ($\mathbf{1}^+$ to **1H**). However, part of the change is due to the irreversible reduction of a species other than $\mathbf{1}^+$ in the presence of sodium pyruvate, evidenced by an offset in the convolution integral of ~0.5 mM from the baseline after both oxidation events. With sodium pyruvate, the concentration changes after *ox1* and *ox2* are roughly equal, showing that the concentrations of $\mathbf{1}_{\mathbf{dim}}$ and **1H** are approximately the same after the reduction event (corresponding to ~30% selectivity for **1H** formation).

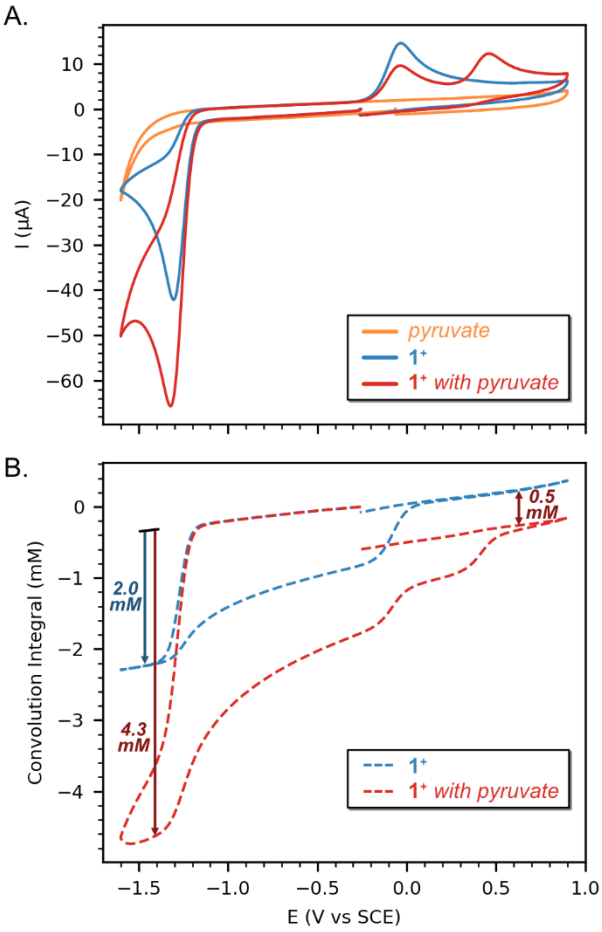


**Figure 2.** (A) Representative cyclic voltammograms and (B) the corresponding convolution integrals of 2 mM **1**$^{+}$ in the absence (—) or presence (—) of 100 mM sodium pyruvate, or 100 mM sodium pyruvate alone (—). Experiments were performed using a 2 mm boron doped diamond working electrode with 100 mM sodium phosphate supporting electrolyte purged with $N_2$ and at pH 7.0, 25 °C and 800 mV $s^{-1}$.

To better understand the mechanism of action of sodium pyruvate, we studied the dependence of **1**$^{+}$ reduction on the concentration of pyruvate, the reduction potential, and the pH of the solution. Voltammetry of **1**$^{+}$ with variable pyruvate concentration (using sodium bicarbonate as a co-supporting electrolyte to maintain a total supporting electrolyte concentration of 200 mM) revealed that trace amounts of **1H** are formed with as little as 2 mM sodium pyruvate (1 eq. with respect to **1**$^{+}$) (Figure 3). Although raising the concentration of sodium pyruvate increased the yield of **1H** at low pyruvate concentrations, too much sodium pyruvate was detrimental to the yield of **1H**. For example, a 50:50 mixture of sodium bicarbonate/sodium pyruvate yielded more **1H** than sodium pyruvate alone, which might suggest a synergistic interaction between pyruvate and

the co-supporting electrolyte. A similar result was also observed with a 50/50 mixture of sodium phosphate/sodium pyruvate, which yielded more **1H** than sodium pyruvate alone.

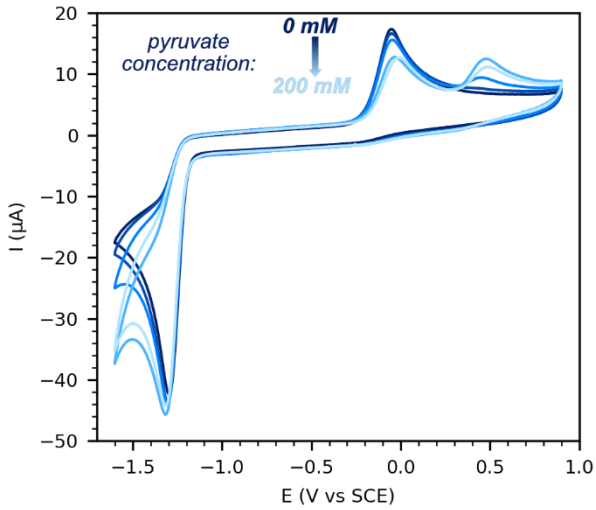


**Figure 3.** Representative cyclic voltammograms of 2 mM $\mathbf{1}^{+}$ with varying ratios of sodium bicarbonate/sodium pyruvate: 100/0 (darkest), 99/1, 90/10, 50/50, and 0/100 (lightest). Experiments were performed using a 2 mm boron doped diamond working electrode at 25 °C and 800 mV $s^{-1}$. Solutions were purged with nitrogen before scanning.

We next sought to determine the impact of switching potential on the peak currents corresponding to *ox1* and *ox2* ($i_{pa1}$ and $i_{pa2}$, respectively) exhibited in CVs of $\mathbf{1}^{+}$. In sodium pyruvate (200 mM, pH 7.0), both $\mathbf{1}_{\mathbf{dim}}$ and **1H** are formed in the same reduction event, with **1H** favored at lower potentials and $\mathbf{1}_{\mathbf{dim}}$ favored at higher potentials (Figure 4a). At a turnaround potential of -1.25 V (green curve), only a trace amount of $\mathbf{1}^{+}$ is generated during *ox2*, but this amount grows significantly as the potential is lowered to -1.6 V (blue curve). By contrast, the amount of $\mathbf{1}^{+}$ generated during *ox1* grows more slowly at lower turnaround potentials. Without sodium pyruvate (200 mM sodium phosphate, pH 9.1), no observable **1H** is formed by -1.6 V. Additionally, there is minimal change in product distribution between -1.6 V and -2.1 V (Figure 4). Below -2.1 V, the product distribution shifts away from dimer, yet **1H** is not formed exclusively: at least three new oxidation peaks are observed, and dimer is still the major product. The comparison of these two electrolytes shows a general pH dependence for the electrochemical reduction of $\mathbf{1}^{+}$ to **1H**, a reaction that happens both more selectively and more quickly with sodium pyruvate than without it.

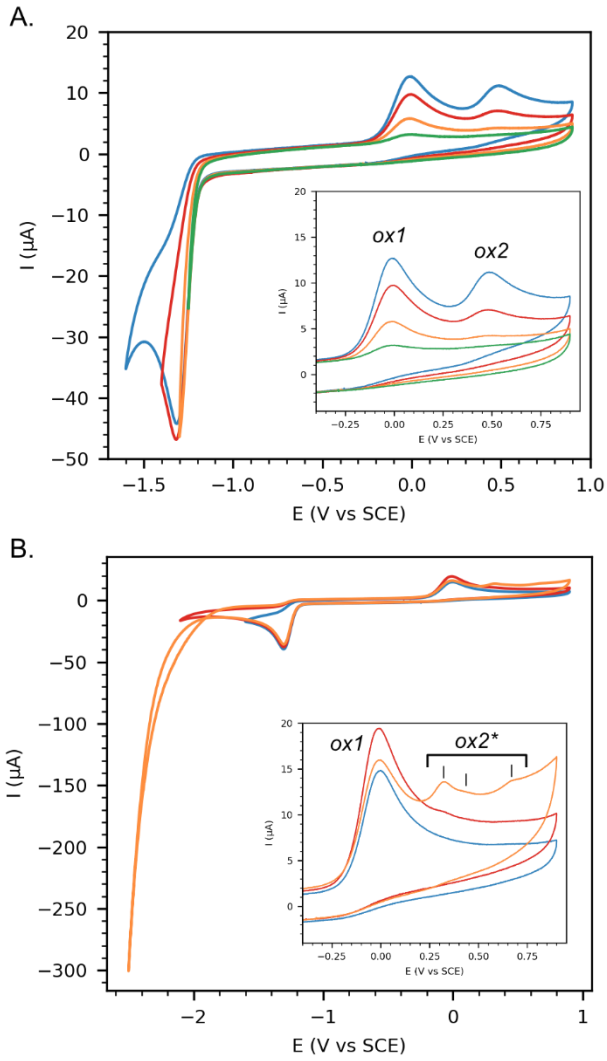


**Figure 4.** (A) Representative cyclic voltammograms of 2 mM **1**$^{+}$ with 200 mM sodium pyruvate with variable turnaround potentials: -1.6 V (—), -1.4 V (—), -1.3 V (—), and -1.25 V (—). (B) Representative cyclic voltammograms of 2 mM **1**$^{+}$ with 200 mM $Na_2HPO_4$ with different turnaround potentials: -1.6 V (—), -2.1 V (—), and -2.5 V (—). Experiments were performed using a 2 mm boron doped diamond working electrode at 25 °C and 800 mV $s^{-1}$. Solutions were purged with nitrogen before scanning.

We also explored the pH dependence of **1**$^{+}$ reduction in 100 mM sodium phosphate, with and without 100 mM sodium pyruvate. In the absence of pyruvate, the peak current for *ox1* changed weakly with pH, and only trace evidence of *ox2* was observed at more acidic pH (see Table 1 above). Under neutral or slightly basic conditions, there was no impact on the reduction peak and only *ox1* was observed. In slightly acidic solutions, a small oxidation peak near 0.38 V

could be seen; however, this peak represents a negligible fraction of the total products formed during the electrochemical reduction of **1**$^{+}$. In the presence of 100 mM sodium pyruvate, by contrast, the peak reduction current had a pronounced pH dependence (Figure 5A, $i_{pc}$ grows from 43 μA at pH 9 to 112 μA at pH 5). The two-electron product **1H** was clearly visible at every pH, although the product ratio **1H**:**1**$_{dim}$ exhibited a maximum value at pH 7 (Figure 5B). At more basic pH, the formation of **1H** increased with the peak reduction current, but at more acidic pH, even though the peak reduction current continued to grow, the amount of **1H** fell and dimer was again the major product. It should be noted that the sum of $i_{pa1}$ and $i_{pa2}$ at each pH was nearly unchanged; assuming the diffusivities of **1**$_{dim}$ and **1H** are independent of pH, this suggests that **1*** is reacting via only two competitive reaction pathways, one pathway that forms **1**$_{dim}$ and one that forms **1H**. The decrease in *ox1* at pH 5 may be due to acid-promoted decomposition of the dimer; for example, the dimer of 1-methyl nicotinamide has a first-order decomposition rate constant of 6400 $s^{-1}$ at pH 4.4.[24]

While the total amount of **1H** and **1**$_{dim}$ formed is approximately constant as the pH is lowered from 9 to 5, the peak reduction current continues to increase, showing that that the reduction of the species other than **1**$^{+}$ (described as causing the offset of 0.5 M in the convolution integral in Figure 2B above) is acid-promoted. Additionally, the pH maximum for **1H** formation indicates that the competing reduction event has a higher-order dependence on proton concentration than the reduction of **1**$^{+}$ to **1H**, because its rate grows more rapidly with proton concentration than the rate of formation of **1H**. Further inspection of the CVs with and without sodium pyruvate indicates that this competing reaction may be pyruvate reduction. Control experiments indicate that sodium pyruvate is electrochemically active, with a peak reduction potential of -2.2 V at 400 mV/s in pH 7 phosphate buffer. Although this potential is well beyond the -1.6 V cutoff for the CVs of **1**$^{+}$ shown here, the onset of the pyruvate reduction wave is still visible in background scans (this can be seen in Figure 2 above). An alternative explanation is that a synergistic interaction between **1**$^{+}$ and pyruvate may enable electrocatalytic proton reduction. However, we could not observe an interaction between sodium pyruvate and **1**$^{+}$ in bulk solution by $^{1}$H-NMR (see Supporting Information). Ongoing research is aimed at understanding this secondary reaction/interaction.

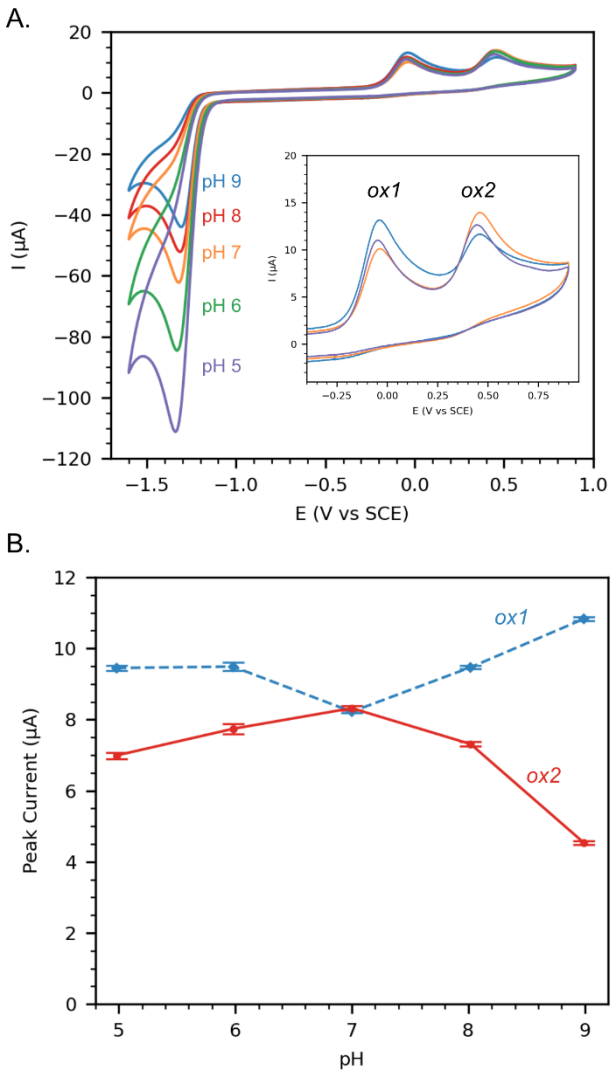


**Figure 5.** (A) Representative cyclic voltammograms of 2 mM $\mathbf{1}^{+}$ in 100 mM sodium phosphate with 100 mM sodium pyruvate, at pH 9 (—), 8 (—), 7 (—), 6 (—), and 5 (—). (B) Normalized peak currents for *ox1* and *ox2* at the same pH values, showing a maximum of *ox2* (**1H**) and a minimum of *ox1* ($\mathbf{1}_{\mathbf{dim}}$) at pH 7. Error bars represent one standard deviation from the mean where $n$ = 3. Experiments were performed using a 2 mm boron doped diamond working electrode at 25 °C and 800 mV $s^{-1}$. Solutions were purged with nitrogen before scanning.

Finally, we explored the ability for other pyridinium electrolytes to be regenerated by sodium pyruvate. To that end, we varied the 1-substituent to include ethyl (**2**), isopropyl (**3**),and allyl (**4**) derivatives, as well as $NAD^{+}$ itself (**5**). All of these pyridinium compounds showed both *ox1* and *ox2* in a mixture of 100 mM sodium phosphate and 100 mM sodium pyruvate (pH 7). The effect of sodium pyruvate was most pronounced for the substrate with the smallest 1-substituent,

1-ethyl nicotinamide bromide (**2**), and it was least pronounced for the substrate with the largest 1-substituent, $NAD^+$ (**5**). Although the 1-substituent can have a significant effect on the extent of interaction between pyruvate and the pyridinium electrolyte, the interaction appears to be general for nicotinamide-based electrolytes, suggesting that the ability of pyruvate to promote the electrochemical generation of **1H** from $\mathbf{1}^+$ presents a general strategy for direct electrochemical regeneration of NADH analogues and NADH itself.

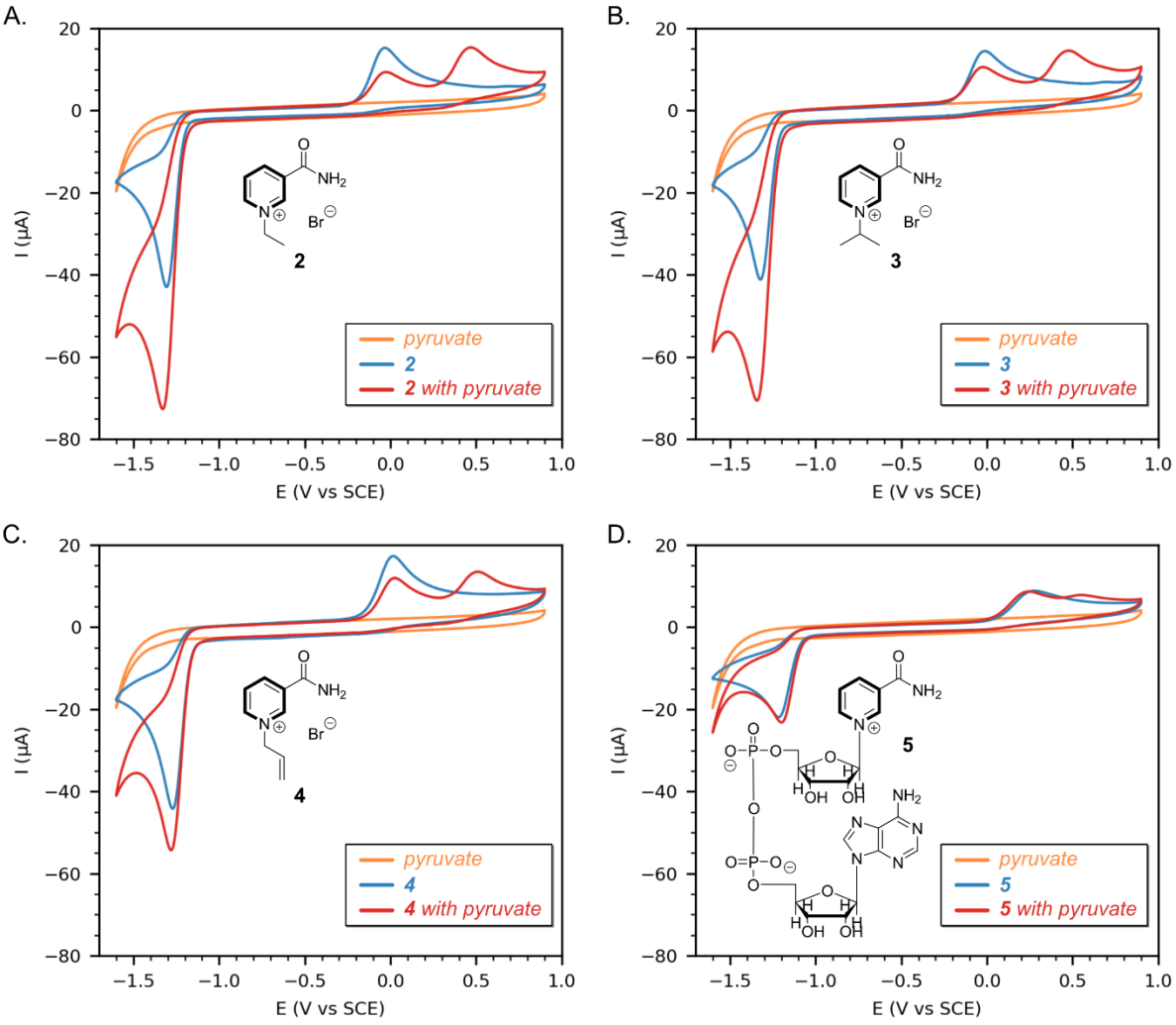


**Figure 5.** Representative cyclic voltammograms of 2 mM pyridinium electrolyte in 100 mM sodium phosphate in the presence (—) or absence (—) of 100 mM sodium pyruvate, or 100 mM sodium pyruvate alone (—): (A) 1-ethyl nicotinamide bromide, **2**; (B) 1-isopropyl nicotinamide bromide, **3**; (C) 1-allyl nicotinamide bromide, **4**; (D) nicotinamide adenine dinucleotide, **5**. Experiments were performed using a 2 mm boron doped diamond working electrode at 25 °C and 800 mV $s^{-1}$. Solutions were purged with nitrogen before scanning.

## CONCLUSIONS

We screened the electrochemical reduction of 1-*n*-butyl nicotinamide bromide (**1**$^+$) in 28 different supporting electrolytes and compared against the electrochemical oxidation of 1,4-dihydro-1-*n*-butyl nicotinamide (**1H**). While **1**$^+$ reduction yielded only dimer in most of the electrolytes tested, sodium pyruvate gave rise to a significant amount of **1H** alongside the dimer. The interaction with sodium pyruvate is optimized when a large excess of sodium pyruvate is combined with a large excess of a co-supporting electrolyte, such as bicarbonate or phosphate. The interaction with pyruvate is also favored at low potentials and at neutral pH; however, it could not be observed in bulk solution by $^1$H-NMR. Several different pyridinium electrolytes, including NAD$^+$, are susceptible to the interaction with sodium pyruvate, suggesting that addition of sodium pyruvate can be a general strategy for regenerating NADH analogues and NADH itself from their oxidized forms.

## EXPERIMENTAL PROCEDURES

*Synthesis:*

*1-n-butyl-3-carbamoylpyridinium bromide (1$^+$)*: Nicotinamide (1.235 g, 10.1 mmol), acetonitrile (10 mL), 1-bromobutane (2.15 mL, 20 mmol), and a stir bar were added to a 20 mL scintillation vial with a pressure release cap. The mixture was stirred at 50 °C for 2 h and then at 80-100 °C for 10 h. The contents were quantitatively transferred with ethanol to a 100 mL round bottom flask, and the solvent was removed in vacuo. The soapy residue was crystallized from cyclohexane/ethanol to afford the product as white crystals (1.457 g, 56%).

*1-n-butyl-1,4-dihydronicotinamide (1H)*: Adapted from a previous procedure[5]. Water (10 mL), dichloromethane (5 mL), sodium bicarbonate (390 mg, 4.6 mmol), and and mNAD$^+$ (200 mg, 0.77 mmol) were added to a 25 mL round bottom flask with a stir bar. Dry sodium dithionite (540 mg, 3.1 mmol) was added to an addition funnel, which was clipped to the top of the flask and sealed with a rubber stopper. The flask was lowered into an ice bath, and the contents were mixed while a Schlenk line was used to remove oxygen from the system. The addition funnel was opened and the dithionite added slowly over 10-15 min. After mixing for 2 h in the dark, the organic layer was washed three times with cold water, dried over $MgSO_4$, and concentrated in vacuo to yield the title product as a yellow-orange, semicrystalline residue (25 mg, 18%).

*1-allyl-3-carbamoylpyridinium bromide*: Nicotinamide (1.241 g, 10.2 mmol), acetonitrile (10 mL), allyl bromide (0.840 mL, 9.9 mmol), and a stir bar were added to a 20 mL scintillation vial with a pressure-release cap. The mixture was stirred at 50 °C for 12 h. The contents were quantitatively

transferred with ethanol to a 100 mL round bottom flask, and the solvent was removed in vacuo. The solid was recrystallized from ethanol/hexanes to afford the product as a light brown crystalline solid (1.509 g, 61%).

*1-isopropyl-3-carbamoylpyridinium bromide*: Nicotinamide (122.5 mg, 1.00 mmol), 2-bromopropane (0.1878 mL, 2.00 mmol), and acetonitrile (2 mL) were added to a Parr bomb reactor, and the contents were heated at 100 °C for 24 h. After cooling, the contents were quantitatively transferred with methanol to a round-bottom flask, the solvent was boiled away, and the residue was recrystallized from ethanol/hexanes to afford the product as a white powder (84.3 mg, 34%).

*Electrochemistry:*

Unless otherwise noted, supporting electrolyte solutions were prepared by dissolving 2.00 mmol of electrolyte in a small amount of water and diluting to 10.0 mL. (Heat was needed to dissolve sodium tetraborate decahydrate). Solutions of sodium acetate and sodium propionate were prepared by combining equal amounts of the acid and sodium bicarbonate.

For electrochemical testing, 6 µmol (1.55 mg for **1**$^{+}$, 1.08 mg for **1H**) of substrate was added to a 10 mL glass beaker and dissolved in 3 mL of supporting electrolyte solution (the volume was scaled accordingly if more or less substrate was added). The solution was purged with nitrogen for several minutes before scanning and for ~10 seconds between scans. The electrodes were boron-doped-diamond (working), saturated calomel (reference), and platinum wire (counter). Unless otherwise noted, scans were run at 800 mV/s between -1.6 V and 0.9 V, starting from the open circuit potential.

**ACKNOWLEDGEMENTS**

The authors wish to acknowledge the ACS Petroleum Research Fund (PRF #65477-DNI4) for their support of this research.

**REFERENCES**

(1) Chen, H.; Dong, F.; Minteer, S. D. The Progress and Outlook of Bioelectrocatalysis for the Production of Chemicals, Fuels and Materials. *Nature Catalysis*. Nature Research March 1, 2020, pp 225–244. https://doi.org/10.1038/s41929-019-0408-2.

(2) Sellés Vidal, L.; Kelly, C. L.; Mordaka, P. M.; Heap, J. T. Review of NAD(P)H-Dependent Oxidoreductases: Properties, Engineering and Application. *Biochimica et Biophysica Acta - Proteins and Proteomics*. Elsevier B.V. February 1, 2018, pp 327–347. https://doi.org/10.1016/j.bbapap.2017.11.005.

(3) Löw, S. A.; Löw, I. M.; Weissenborn, M. J.; Hauer, B. Enhanced Ene-Reductase Activity through Alteration of Artificial Nicotinamide Cofactor Substituents. *ChemCatChem* **2016**, *8* (5), 911–915. https://doi.org/10.1002/cctc.201501230.

(4) Paul, C. E.; Arends, I. W. C. E.; Hollmann, F. Is Simpler Better? Synthetic Nicotinamide Cofactor Analogues for Redox Chemistry. *ACS Catalysis*. March 7, 2014, pp 788–797. https://doi.org/10.1021/cs4011056.

(5) Paul, C. E.; Gargiulo, S.; Opperman, D. J.; Lavandera, I.; Gotor-Fernández, V.; Gotor, V.; Taglieber, A.; Arends, I. W. C. E.; Hollmann, F. Mimicking Nature: Synthetic Nicotinamide Cofactors for C=C Bioreduction Using Enoate Reductases. *Org Lett* **2013**, *15* (1), 180–183. https://doi.org/10.1021/ol303240a.

(6) Lutz, J.; Hollmann, F.; Ho, T. V.; Schnyder, A.; Fish, R. H.; Schmid, A. Bioorganometallic Chemistry: Biocatalytic Oxidation Reactions with Biomimetic NAD+/NADH Co-Factors and [Cp*Rh(Bpy)H]+ for Selective Organic Synthesis. In *Journal of Organometallic Chemistry*; Elsevier B.V., 2004; Vol. 689, pp 4783–4790. https://doi.org/10.1016/j.jorganchem.2004.09.044.

(7) Ryan, J. D.; Fish, R. H.; Clark, D. S. Engineering Cytochrome P450 Enzymes for Improved Activity towards Biomimetic 1,4-NADH Cofactors. *Chembiochem* **2008**, *9* (16), 2579–2582. https://doi.org/10.1002/cbic.200800246.

(8) Jensen, M. A.; Elving, P. J. Nicotinamide Adenine Dinucleotide (NAD+). Formal Potential of the NAD+/NAD· Couple and NAD· Dimerization Rate. *Biochimica et Biophysica Acta (BBA) - Bioenergetics* **1984**, *764* (3), 310–315. https://doi.org/10.1016/0005-2728(84)90101-4.

(9) Elving, P. J.; Bresnahan, W. T.; Moiroux, J.; Samec, Z. 524—NAD/NADH as a Model Redox System: Mechanism, Mediation, Modification by the Environment. *J Electroanal Chem Interfacial Electrochem* **1982**, *141* (3), 365–378. https://doi.org/10.1016/0022-0728(82)85223-6.

(10) Burnett, J. N.; Underwood, A. L. Electrochemical Reduction of 1-Methyl-3-Carbamidopyridinium Chloride. *Journal of Organic Chemistry* **1965**, *30*, 1154–1158.

(11) Hollmann, F.; Schmid, A.; Steckhan, E. The First Synthetic Application of a Monooxygenase Employing Indirect Electrochemical NADH Regeneration. *Angew. Chem. Int. Ed* **2001**, *40* (1).

(12) Ali, I.; Gill, A.; Omanovic, S. Direct Electrochemical Regeneration of the Enzymatic Cofactor 1,4-NADH Employing Nano-Patterned Glassy Carbon/Pt and Glassy Carbon/Ni Electrodes. *Chemical Engineering Journal* **2012**, *188*, 173–180. https://doi.org/10.1016/j.cej.2012.02.005.

(13) Kaneco, S.; Iiba, K.; Yabuuchi, M.; Nishio, N.; Ohnishi, H.; Katsumata, H.; Suzuki, T.; Ohta, K. High Efficiency Electrochemical CO2-to-Methane Conversion Method Using Methanol with Lithium Supporting Electrolytes. *Ind Eng Chem Res* **2002**, *41* (21), 5165–5170. https://doi.org/10.1021/ie0200454.

(14) Stone, N. J.; Swelgart, D. A.; Bond, A. M. Effects of Temperature and Supporting Electrolyte on the Electrochemical Oxidation of (Benzene)Tricarbonylchromium and Other

π Hydrocarbon Complexes. *Organometallics* **1986**, *5*, 2553–2555. https://doi.org/10.1021/om00143a027.

(15) L J. Duić; Z. Mandić; F. Kovačiček. The Effect of Supporting Electrolyte on the Electrochemical Synthesis, Morphology, and Conductivity of Polyaniline. *J Polym Sci A Polym Chem* **1994**, *32*, 105–111. https://doi.org/10.1002/pola.1994.080320112.

(16) Katsounaros, I.; Kyriacou, G. Influence of the Concentration and the Nature of the Supporting Electrolyte on the Electrochemical Reduction of Nitrate on Tin Cathode. *Electrochim Acta* **2007**, *52* (23), 6412–6420. https://doi.org/10.1016/j.electacta.2007.04.050.

(17) Peters, B. K.; Rodriguez, K. X.; Reisberg, S. H.; Beil, S. B.; Hickey, D. P.; Kawamata, Y.; Collins, M.; Starr, J.; Chen, L.; Udyavara, S.; Klunder, K.; Gorey, T. J.; Anderson, S. L.; Neurock, M.; Minteer, S. D.; Baran, P. S. Scalable and Safe Synthetic Organic Electroreduction Inspired by Li-Ion Battery Chemistry. *Science (1979)* **2019**, *363* (6429), 838–845. https://doi.org/10.1126/science.aav5606.

(18) Murray, R. W.; Hiller, L. K. Supporting Electrolyte Effects in Nonaqueous Electrochemistry Coordinative Relaxation Reactions of Reduced Metal Acetylacetonates in Acetonitrile. *Anal Chem* **1967**, *39* (11), 1221–1229. https://doi.org/10.1021/AC60255A011/ASSET/AC60255A011.FP.PNG_V03.

(19) Elving, P. J.; Milazzo, ; G; Dryhurst, ; G; Moiroux, ; J; Jensen, ; A J; Ohnishi, ; Y; Kikuchi, Y.; Kitami, M. The Role of Adsorption in the Initial One-Electron Electrochemical Reduction of Nicotinamide Adenine Dinucleotide (NAD+). *J Am Chem Soc* **1981**, *103* (9), 2379–2386.

(20) Schmakel, C. O.; Santhanam, K. S. v.; Elving, P. J. Nicotinamide and N'-Methylnicotinamide: Electrochemical Redox Pattern: Behavior of Free Radical, Dimeric, and Dihydropyridine Species. *J Electrochem Soc* **1974**, *121* (3), 345. https://doi.org/10.1149/1.2401814.

(21) Oldham, K. B.; Spanier, J. The Replacement of Fick's Laws by a Formulation Involving Semidifferentiation. *J Electroanal Chem Interfacial Electrochem* **1970**, *26* (2–3), 331–341. https://doi.org/10.1016/S0022-0728(70)80316-3.

(22) Oldham, K. B. A Signal-Independent Electroanalytical Method. *Anal Chem* **1972**, *44* (1), 196–198. https://doi.org/10.1021/ac60309a028.

(23) Imbeaux, J. C.; Savéant, J. M. Convolutive Potential Sweep Voltammetry: I. Introduction. *J Electroanal Chem Interfacial Electrochem* **1973**, *44* (2), 169–187. https://doi.org/10.1016/S0022-0728(73)80244-X.

(24) Miller, M.; Czochralska, B.; Shugar, D. Red-Ox Transformations of NAD+ Model Compounds. *J Electroanal Chem Interfacial Electrochem* **1982**, *141* (3), 287–298. https://doi.org/10.1016/0022-0728(82)85215-7.